Very long-term stability of passive margin escarpment constrained by 40 Ar-39 Ar dating of K-Mn oxides

Anicet Beauvais, Nicolas J. Bonnet, Dominique Chardon, Nicolas Olivier Arnaud, Mudlappa J Jayananda

Very long-term stability of passive margin escarpment constrained by ^{40}Ar-^{39}Ar dating of K-Mn oxides

Anicet Beauvais [1*], Nicolas J. Bonnet [1], Dominique Chardon [2, 3, 4], Nicolas Arnaud [5], Mudlappa Jayananda [6]

[1] Aix-Marseille Université (AMU), IRD, CNRS, CEREGE UM34, BP 80, 13545 Aix-en-Provence, Cedex 4, France

[2] IRD, UR 234, GET, 14 Avenue Edouard Belin, 31400 Toulouse, France

[3] Université de Toulouse, UPS (OMP), 31400 Toulouse, France

[4] CNRS, GET, 31400 Toulouse, France

[5] Université de Montpellier 2, Géosciences Montpellier, UMR CNRS 5243, 34095 Montpellier, France

[6] Centre for Earth and Space Sciences, University of Hyderabad, P.O Central University Gachibowli, Hyderabad 500 046, India

*Corresponding author: Anicet Beauvais (beauvais@cerege.fr)

Submitted to **Geology**, August 27th, 2015

ABSTRACT

The post-rift denudation history of high-elevation divergent continental margins is central to decipher "source-to-sink" systems across such margins and to unravel the topographic evolution of their escarpment. We perform ^{40}Ar-^{39}Ar dating of supergene cryptomelane (K-Mn oxide) from supergene manganese ore deposits to constrain the age of in-situ formed laterites of the low-relief lowland and highland separated by the Western Ghats Escarpment (WGE) of Peninsular India. Documentation of laterites as old as 53 Ma on the highland and 47 Ma at the foot of the WGE shows that the escarpment stabilized before 47 Ma (possibly 60 Ma ago). The geomorphic setting of the dated weathering mantles further allows constraining post-Early Eocene denudation of the lowland and the highland to maximums of 5 and 15 m/My, respectively. These results allow refining apatite fission track thermochronology and cosmogenic radionuclides studies that overestimate 4 to 20 times denudation rates, particularly after escarpment stabilization.

INTRODUCTION

Constraining the denudation history of high elevation (i.e., escarpment bearing) divergent continental margins documents their post-rift topographic evolution that has implications to quantify their vertical motion, drainage pattern and sedimentary supply over geological time scales. Current evolution models of high-elevation passive margin topography predict contrasted denudation histories. Models based on apatite fission track thermochronology (AFTT) predict a short period (≤ 10-15 Ma) of high denudation focused on a coastal strip resulting in escarpment formation shortly after the onset of rifting (Brown et al., 2002; Braun and van der Beek, 2004; see also Matmon et al.,

2002). An alternative model integrating AFTT, the elevation of paleosurfaces and indirect geological constraints argues for successive burials, uplifts and topographic rejuvenations after continental break-up implying that escarpments result from the last uplift episode (Japsen et al., 2012). However, possible thermal instabilities in the shallow crust (< 2 km, i.e., T°< 60°C) and the failure of AFTT models to quantify erosion of crustal sections < 1 km (Brown and Summerfield, 1997) result in large uncertainties in the timing and magnitude of denudation predicted by these models (see also Kohn et al., 2005). Whether and how escarpments are rejuvenated after their formation (e.g., Moore and Blenkinsop, 2006) is also debated because the mode and velocity of their retreat have crucial implications on the evolution of the drainage networks of continental margins and their sedimentary budgets (e.g., Tucker and Slingerland, 1994). Studies based on cosmogenic radionuclides (CRN) predict slow denudation and retreat of escarpments, i.e., 3 to 16 m/My (Bierman and Caffee, 2001), but are only valid over millennial time scales.

Once slow denudation regimes (< 20 m/My) install on continental margins, remnant landscapes may be commonly preserved as a result of limited to moderate relief inversion (Beauvais and Chardon, 2013). In the tropical belt, such paleolandscape remnants are mantled by laterites that may host K-Mn oxydes (cryptomelane) datable by $^{40}Ar/^{39}Ar$ geochronology that already proved beneficial (e.g., Vasconcelos, 1999; Vasconcelos and Conroy, 2003; Beauvais et al., 2008). If properly mapped and dated, lateritic paleolandscape remnants are very useful to calibrate erosion over geological time scales (Beauvais and Chardon, 2013). Here we combine geomorphology with the dating of cryptomelane from in-situ formed lateritic Mn ore deposits preserved at the foot and above the Western Ghats Escarpment (WGE) of Peninsular India as a test of

post break-up denudation scenarios deduced from AFTT and CRN studies (Gunnell et al., 2003; Mandal et al., 2015). Our results lead to very low denudation rates (< 5-15 m/My) since stabilization of the escarpment at least 50 Ma ago and argue for a great stability of both the topography and relief of the margin since then.

GEOMORPHOLOGICAL AND GEOCHRONOLOGICAL OUTLINES

The WGE is up to 1000 m high and was carved into the Deccan traps and their Archean basement (Fig. 1a). The escarpment separates the coastal lowland from the highland plateau and coincides with the continental divide along most of its trace (Fig. 1a). The lowland consists of a weakly dissected lateritic pediment (Figs. 1b and 1c) making the seaward piedmont of the WGE (Widdowson and Gunnell, 1999), on which laterites have been loosely dated to Mid- and Late Tertiary by paleomagnetism (Schmidt et al., 1983). The poorly defined highland laterites would have Late Cretaceous-Eocene paleomagnetic ages (Schmidt et al., 1983). Those laterites are mostly bauxites and mantle a low-relief relict landscape best preserved as 1000-1100 m high mesas near the WGE (e.g., Krishna Rao et al. 1989). Within the highland plateau, relicts of that paleolandscape are sparser (Fig. 1b). At Sandur, ^{40}Ar-^{39}Ar dating of supergene cryptomelane formed in Mn ore deposits carried by such an highland relict (Figs. 1a and 1b) documents a period of intense lateritic weathering at c. 36-26 Ma (Bonnet et al., 2014), after the formation of Eocene bauxites (Krishna Rao et al., 1989) and before Neogene landscape dissection (Radhakrishna, 1993).

Inversion of apatite fission track data predicts higher denudation in the lowland (up to 120 m/My) than in the highland (< 20 m/My) between 80 and 50 Ma, and low (< 20 m/My) denudation on either side of the escarpment after 40 Ma (Gunnell et al.,

2003). This suggests that the WGE formed at c. 50 Ma, after the extrusion of Deccan traps (65 ± 2 Ma) and largely after rifting between India and Madagascar (88 ± 3 Ma).

FIELD RELATIONSHIPS, MATERIAL AND METHOD

The lowland pediment consists of a c. 40 km wide concave surface ranging in elevation from 30 to 300 m, and incised by 25 to 100 m deep valleys (Figs. 1b-c). Field observations indicate that the pediment has truncated a bauxitic profile before being in turn weathered and cemented by a ferricrete, which caps a 25 to 60 m thick lateritic weathering profile (Fig. 1c). The studied lowland Caurem and Naveli Mn ore deposits are lentoid pockets within the pediment weathering profiles developed from Archean manganiferous schists and phyllites. The two open cast pits are located at the foot of the WGE at ~ 100 m and 140 m elevation, respectively (Fig. 1c), and four samples were collected at altitudes of 68 m and 45 m in Caurem pit and 113 m and 85 m in Naveli pit (see supplemental material). The highland Sandur Mn ore deposit formed upon Archean manganiferous phyllites and is exposed on a relict lateritic paleosurface capped by a ferricrete at 1012-1015 m elevation (Fig. 1b). Two samples were collected on benches at altitudes of 890 to 975 m (see supplemental material). All samples are massive with botryoidal or cavity filling structures enabling cryptomelane crystallization.

Thorough optical microscopy and X-ray micro-fluorescence analyses of 200-300 μm thin sections allowed separation of eight cryptomelane grains from 300-500 μm symmetrical sections slabs using a binocular magnifier (see Bonnet et al., 2014). The separated grains were characterized using X-ray diffraction, electron microprobe analyses and scanning electron microscopy before irradiation. Cryptomelane ($K_xMn^{IV}_{8-x}Mn^{III}_xO_{16}$) crystallizes into a monoclinic prismatic system with a typical tunnel-type

121 crystal lattice framed by a double chain of MnO_6 octahedra and K^+ cations in the large
122 tunnel to insure the electronic neutrality of the lattice (Turner and Buseck, 1979). High
123 retentiveness of potassium (content up to 5.5 wt.% K) and radiogenic argon ($^{40}Ar^*$) in
124 the intra-crystalline tunnels warranties the suitability of cryptomelane for ^{40}Ar-^{39}Ar
125 dating (see Vasconcelos, 1999).
126 Gas was extracted from the irradiated cryptomelane grains either from a step-wise
127 heating procedure in a double staudacher-type furnace, or from step incremental heating
128 of the grains with a CO_2 laser probe power. The gas fractions were then cleaned and
129 analyzed using a VG3600 or Argus IV mass spectrometer. The $^{40}Ar/^{39}Ar$ ages are
130 calculated from plateaus encompassing at least three consecutive ^{39}Ar release steps
131 comprising up to 50% of total $^{39}Ar_K$ released, and from best-fit inverse isochrones in
132 $^{36}Ar/^{40}Ar$ vs. $^{39}Ar/^{40}Ar$ correlation diagrams (see also supplemental material).
133
134 **RESULTS AND INTERPRETATIONS**
135 The ^{39}Ar release spectra of irradiated cryptomelane grains are stacked in the
136 Figures 2a and 2b. Each age spectrum allows calculation of a precise age from a plateau
137 encompassing heating steps overlapping at 2σ confidence level while degassing at least
138 5% of the total ^{39}Ar released from the highly retentive intra-crystalline sites of
139 cryptomelane structure. The calculated plateau ages also agree well with the isochron
140 ages (Table 1; see also data repositories DR1 to DR2 in supplemental material). The
141 ^{40}Ar-^{39}Ar ages from the highland Sandur deposit document a weathering period from c.
142 53 to c. 50 Ma (Fig. 2a and 2c). These ages complement those previously obtained in
143 the same deposit from c. 36 to c. 26 Ma by Bonnet et al. (2014), which are also shown
144 in figures 2a and 2c. The old ages (53-50 Ma) in the highland are interpreted to reflect

(bauxitic) weathering of the low-relief relict landscape, whereas the 36-26 Ma weathering period (Bonnet et al., 2014) is interpreted as that having led to the geochemical reworking of the bauxites documented by Krishna Rao et al. (1989). Lateritic profiles of the lowland pediment record weathering periods at c. 47-45 Ma, c. 24-19 Ma, and an episode at c. 9 Ma (Fig. 2b and 2c). The 47-45 Ma ages date the early (bauxitic) weathering of the lowland, whereas the ages between 24 and 19 Ma document renewed weathering and formation of the pediment's capping ferricrete, the 9 Ma age reflecting a discrete weathering pulse.

DISCUSSION

The preservation of in-situ formed laterites as old as 53-50 Ma above and 47-45 Ma below the WGE indicates that the current topographic envelope of the SW Indian margin corresponds to a bauxitic paleosurface dating from the Early Eocene, which already included the WGE with its present amplitude (Fig. 3). The 47-45 Ma old laterites at 55 m depth underneath the lowland pediment belong to a bauxitic profile that did not exceed 120 m in thickness (e.g., Bardossy and Aleva, 1990). Even if the lowland bauxitic profile had been totally eroded (i.e., 120 m of stripping), the maximum denudation rate of the piedmont between early (bauxitic) weathering (47 Ma) and abandonment of the pediment (19 Ma) would be lower than 5 m/My. Given that incision of the pediment does not exceed 100 m, the incision rate of the WGE' piedmont is less than 6 m/My over the last 19 Ma. Anyhow, the remarkable preservation of the pediment surface argues for negligible net denudation of the piedmont's envelope after c. 20 Ma (Fig. 1c).

Different ages recorded at a same depth in the lowland weathering profiles indicate that preserved old lateritic mantles of the escarpment piedmont have undergone several weathering episodes under a slow mechanical denudation regime. Preservation of 47 Ma old bauxitic weathering mantles at least 60 m thick thus attests that the current escarpment established at least 47 Ma ago, and did not retreat since then. Therefore, escarpment formation or retreat driven by Neogene rejuvenation of the lowland (e.g., Radhakrishna, 1993; Widdowson and Gunnell, 1999) is excluded.

Topographic inversion of the low-relief bauxitic paleolandscape throughout the highland plateau rarely attains 450 m (e.g., Figs. 1b and 3). Therefore, the ages (53-50 Ma) obtained on laterites mantling this relict landscape imply a post-Early Eocene incision rate of less that 9 m/My over the last 50 Ma. Given the very low preservation rate of the old paleolandscape (Fig. 3), this incision rate approximates the denudation rate (Beauvais and Chardon, 2013). Renewed weathering of the highland during the Oligocene (i.e., 36-26 Ma; Bonnet et al., 2014) did not result in significant denudation of the Eocene landscape (< 100 m at Sandur and Belgaum for instance; Fig. 1a; Krishna Rao et al., 1989 and our own field observations). Therefore, erosion rates up to 15 m/My may be expected on the highland over the last 26 Ma.

Formation of 47 Ma-old lateritic bauxites at the foot of the WGE would be in agreement with the last denudation pulse predicted at c. 50 Ma in the lowland (Fig. 2c) from AFTT inversion model (Gunnell et al., 2003). But this also suggests that the escarpment is even older as bauxitic profiles form slowly at 3 to 10 m/My in contexts of tectonic quiescence and limited denudation (Boulangé et al., 1997). Therefore, if the lowland bauxitic profile comprising 47 Ma-old laterite was 120 m thick, it would have

taken at least 12 My to develop under an escarpment that should have been stabilized at least 60 Ma ago.

Our results imply denudation rates lower than 5 m/My in the lowland for the last 47 Ma, as opposed to 5-20 m/My (between 40 and 0 Ma) and even 20-70 m/My (between 50 and 40 Ma) from the AFTT model (blue curve in Fig. 2c). Even erosion rates of c. 10^{-2} to 10^{-1} m/ky (10-100 m/My) derived from CRN studies in riverine sediments (Mandal et al., 2015) are also questionable given the remarkable preservation of thick weathering profiles as old as 47 Ma on the WGE' piedmont. Likewise, the preservation of c. 100 m thick highland Eocene lateritic profiles formed upon the latest basaltic flow (63 Ma) of the Deccan traps (Widdowson and Gunnell, 1999) would be unlikely under such erosion rates or those (15-25 m/My) derived from AFTT between 53 and 45 Ma (red curve in Fig. 2c). Furthermore, AFTT fails to precisely measure or detect less than 1 km of denudation, which corresponds to the height of most passive margin escarpments. In other words, our results suggest that AFTT- or CRN derived denudation rates are largely overestimated and not realistic once the escarpment there.

Given the early installation of very slow denudation regimes across high-elevation margins such as that of Peninsular India, we suggest that the combination of radiometric dating ($^{40}Ar/^{39}Ar$ of K-Mn oxides, or $^{4}He/^{3}He$ of Fe-oxides) of lateritic landscape remnants with apatite (U-Th)/He thermochronological models be a powerful tool to refine the denudation history of divergent margins of the tropical belt.

CONCLUSION

^{40}Ar-^{39}Ar geochronology of supergene cryptomelane formed in situ in supergene manganese ore deposits on either side of the Western Ghats escarpment indicate the

development and preservation of an Eocene weathering paleolandsurface mantling the escarpment, attesting of its stability since at least 47-50 Ma, and possibly since 60 Ma. The ages obtained also constrain slow denudation rates of the lowland (< 5 m/My) and the highland (< 15 m/My) of the escarpment after its stabilization. Our results allow refining erosion rates estimated from AFTT and show that absolute dating of lateritic paleolandscape markers may accurately constrain post break-up denudation history of passive margins, with important implications on their sediment delivery histories on geological time scales.

Acknowledgements- This work was funded by IFCPAR project 5007-1, the IRD (UR 161) and the CNRS (INSU 2011-CT2). The French Ministry of Research granted N.J.B. with a three years PhD scholarship (ED251, AMU, OSU Pytheas). Two referees are thanked for their comments on an earlier version of the manuscript.

References

Beauvais, A., and Chardon, D., 2013, Modes, tempo, and spatial variability of Cenozoic cratonic denudation: The West African example: Geochem. Geophys. Geosyst., v. 14, p. 1590-1608.

Beauvais, A., Ruffet, G., Hénocque, O., and Colin, F., 2008, Chemical and physical erosion rhythms of the West African Cenozoic morphogenesis: The ^{39}Ar-^{40}Ar dating of supergene K-Mn oxides: J. Geophys. Res., v. 113, F04007.

Bierman, P. R. and Caffee, M., 2001, Slow rates of rock surface erosion and sediment production across the Namib desert and escarpment, southern Africa: Am. J. Sci., v. 301, p. 326–358.

239 Bonnet, N.J., Beauvais, A., Arnaud, N., Chardon, D., and Jayananda, M., 2014, First
240 $^{40}Ar/^{39}Ar$ dating of intense Late Palaeogene lateritic weathering in Peninsular India:
241 Earth Planet. Sci. Lett., v. 386, p. 126–137.
242 Boulangé, B., Ambrosi, J-P., and Nahon, D., 1997, Laterites and bauxites: In Soils &
243 Sediments: Mineralogy and Geochemistry, H. Paquet & N. Clauer, Eds., Springer
244 Berlin, Heidelberg, pp. 49-65.
245 Braun, J., and van der Beek, P., 2004, Evolution of passive margin escarpments: what
246 can we learn from low-temperature thermochronology?: J. Geophys. Res., v. 109,
247 F04009.
248 Brown, R.W., Summerfield, M.A., 1997, Some uncertainties in the derivation of rates
249 of denudation from thermochronological data: Earth Surf. Proc. Landf., v. 22, 239-
250 248.
251 Brown, R.W., Summerfield, M.A., and Gleadow, A.J.W., 2002, Denudational history
252 along a transect across the Drakensberg escarpment of southern Africa derived from
253 apatite fission track thermochronology: J. Geophys. Research, v. 107, B12, 2350.
254 Campanile, D., Nambiar, C. G., Bishop, P., Widdowson, M., and Brown, R., 2008,
255 Sedimentation record in the Konkan-Kerala basin: implications fro the evolution of
256 the Western Ghats and the Western Indian passive margin: Basin research, v. 20, p.
257 3-22.
258 Chaubey, A.K., Gopala Rao, D., Srinivas, K., Ramprasad, T., Ramana, M.V., and
259 Subrahmanyam, V., 2002, Analyses of multichannel seismic reflection, gravity and
260 magnetic data along a regional profile across the central-western continental margin
261 of India: Marine Geol., v. 182, p. 303-323.

Gunnell, Y., Gallagher, K., Carter, A., Widdowson, M., and Hurford, A.J., 2003, Denudation history of the continental margin of western peninsular India since the early Mesozoic - Reconciling apatite fission-track data with geomorphology: Earth Planet. Sci. Lett., v. 215, p. 187-201.

Japsen, P., Chalmers, J.A., Green, P.F., and Bonow, J.W., 2012, Elevated, passive continental margins: Not rift shoulders, but expressions of episodic, post-rift burial and exhumation: Global Planet. Change, v. 90-91, p. 73-86.

Kohn, B.P., Gleadow, A.J.W., Brown, R.W., Gallagher, K., Lorencak, M., and Noble, W.P., 2005, Visualizing thermotectonic and denudation histories using apatite fission track thermochronology: Rev. Miner. Geochem., v. 58, p. 527-565.

Krishna Rao, B., Satish, P.N., and Sethumadhav, M.S., 1989, Syngenetic and epigenetic features and genesis of the bauxite-bearing laterite of Boknur-Navge, Belgaum district, Karnataka: J. Geol. Soc. India, v. 34, p. 46-60.

Lee J-Y, Marti, K., Severinghaus, J.P., Kawamura, K., Yoo, H-S., Lee, J.B., and Kim, J.S., 2006, A redetermination of the isotopic abundances of atmospheric Ar: Geochim. Cosmochim. Acta, v. 70, 4507–4512.

Mandal, S.K., Lupker, M., Burg, J-P., Valla, P.G., Haghipour, N., and Christl M., 2015, Spatial variability of 10Be-derived erosion rates across the southern peninsular India escarpement: A key to landscape evolution across passive margins: Earth Planet. Sci. Letters, v. 425, p. 154-167.

Matmon, A., Bierman, P., and Enzel, Y., 2002, Pattern and tempo of great escarpment erosion: Geology, v. 30, p. 1135-1138.

Radhakrishna, B.P., 1993, Neogene uplift and geomorphic rejunevation of the Indian Peninsula: Curr. Sci., v. 64, no. 11/12, p. 787-793.

Schmidt, P.W., Prasad, V., and Ramam, P.K., 1983, Magnetic ages of some Indian laterites: Palaeogeogr. Palaeoclimatol. Palaeoecol., v. 44, p. 185–202.

Tucker, G. E., and Slingerland, R. L., 1994, Erosional dynamics, flexural isostasy, and long-lived escarpments: A numerical modeling study: J. Geophys. Res. 99, B6, 12229-12243.

Turner, S., and Buseck, P.R., 1979, Manganese Oxide Tunnel Structures and Their Intergrowths: Science, v. 203, p. 456–458.

Vasconcelos, P.M., 1999, K-Ar and $^{40}Ar/^{39}Ar$ geochronology of weathering processes: Annu. Rev. Earth Planet. Sci., v. 27, p. 183-229.

Vasconcelos, P.M., and Conroy, M., 2003, Geochronology of weathering and landscape evolution, Dugald River valley, NW Queensland, Australia: Geochim. Cosmochim. Acta, v. 67, no. 16, p. 2913-2930.

Widdowson, M., and Gunnell, Y., 1999, Tertiary palaeosurfaces and lateritization of the coastal lowlands of western peninsula India: in Palaeoweathering, Palaeosurfaces and Related Continental Deposits, Thiry, M., and Simon-Coinçon, R., Eds., International Association of Sedimentologists, Sp. Pub., v. 27, p. 245-274.

Whiting, B.M., Karner, G.D., and Driscoll, N.W., 1994, Flexural and stratigraphic development of the West Indian continental margin: J. Geophys. Research, v. 99, p. 13791-13811.

Table caption

Table 1. Plateau and isochrone ages obtained for the cryptomelane separated from samples collected in highland Sandur and lowland Caurem (CAU) and Naveli (NAV) Mn ore pits. Depth indicates the sampling level below the surface. MSWD = Mean

square weight deviation of isochron. ($^{40}Ar/^{36}Ar_{atm}$ = 298.56 ± 0.31 from Lee et al., 2006).

Figures caption

Figure 1. **(a)** Topo-bathymetric setting of the Southwestern Indian margin. **(b)** Topographic cross-section from Sandur to the escarpment edge in the highland and Goa in the lowland (section trace on Fig. 1a). **(c)** Synthetic Cross-section of the lowland piedmont passing through the two dated Mn ore pits.

Figure 2. Stacked ^{40}Ar-^{39}Ar age spectra of cryptomelane from **(a)** the highland and **(b)** the lowland Mn ore pits (located on Fig. 1). **(c)** Weathering periods derived from series of ^{40}Ar-^{39}Ar plateau ages including σ errors, with denudation rate curves derived from inversion model of apatite fission track data (Gunnell et al., 2003), both for the highland (HL) and lowland (LL). (The 36-26 Ma ages are from Bonnet et al., 2014).

Figure 3. Cross-section of the Southwestern Indian divergent margin from offshore basin (A) to Goa, escarpment edge (B) and Sandur (C) (section trace on Fig. 1a). The offshore section including sedimentary limits is adapted from Chaubey et al. (2002), and proportions of clastics are derived from Campanile et al. (2008). Very low offshore accumulation of clastic sediments and correlative Eocene to Mid-Miocene carbonate production (Whiting et al., 1994; Chaubey et al., 2002; Campanile et al., 2008) agrees with onshore weathering and very slow mechanical denudation in the lowland.

Table 1

Sample ID	Depth ± 2 m	Plateau age ± 2σ (Ma)	% ^{39}Ar released	Isochron age ± 2σ (Ma)	^{40}Ar/^{39}Ar intercept ± 2σ	MSWD
Highland						
KMK-2	-37	49.60 ± 1.34	100	49.60 ± 1.41	302.0 ± 25	0.10
KPA-8	-125	53.21 ± 3.43	76	53.01 ± 3.45	296.4 ± 13	0.40
Lowland						
NAV-4	-27	20.84 ± 1.68	54	21.12 ± 0.45	288.0 ± 6	0.33
CAU-1c	-32	21.92 ± 0.23	56	22.07 ± 0.24	294.0 ± 1	2.28
CAU-1a	-32	23.67 ± 0.29	57	23.67 ± 0.29	294.9 ± 2	2.31
NAV-3f	-55	8.65 ± 0.16	84	8.57 ± 0.59	308.7 ± 94	0.55
CAU-3f	-55	19.35 ± 1.52	58	20.22 ± 0.35	283.9 ± 18	0.05
CAU-3a	-55	23.65 ± 0.21	54	23.71 ± 0.21	295.5 ± 2	1.85
NAV-3b	-55	45.08 ± 0.78	57	45.15 ± 0.74	293.7 ± 3	2.04
NAV-3c	-55	47.07 ± 0.54	60	47.11 ± 0.53	293.5 ± 3	1.25

TABLE 1

Figure 1

Click here to download Figure Figure. 1(rev.f).jpg

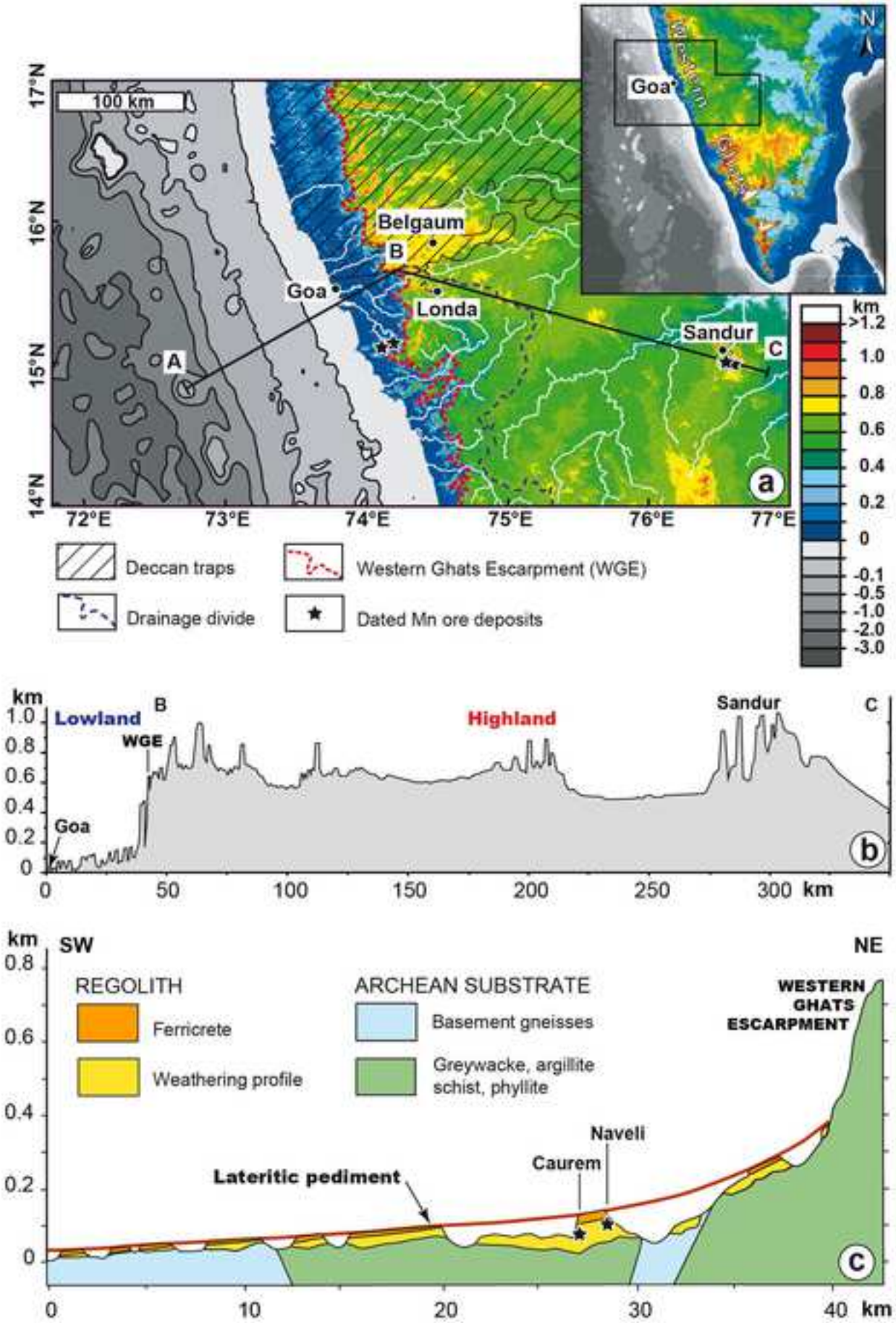

FIGURE 1

Figure 2

Click here to download Figure Figure. 2(rev.f).jpg

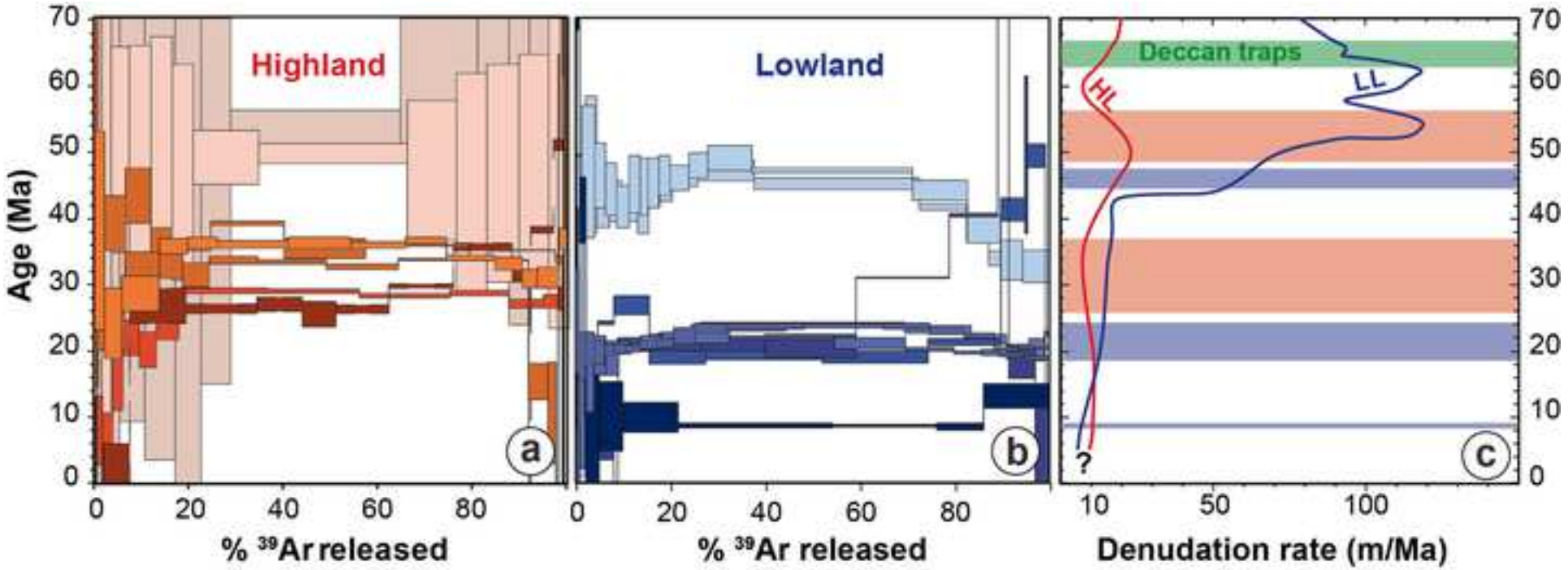

FIGURE. 2

Figure 3

Click here to download Figure Figure. 3(rev.f).jpg

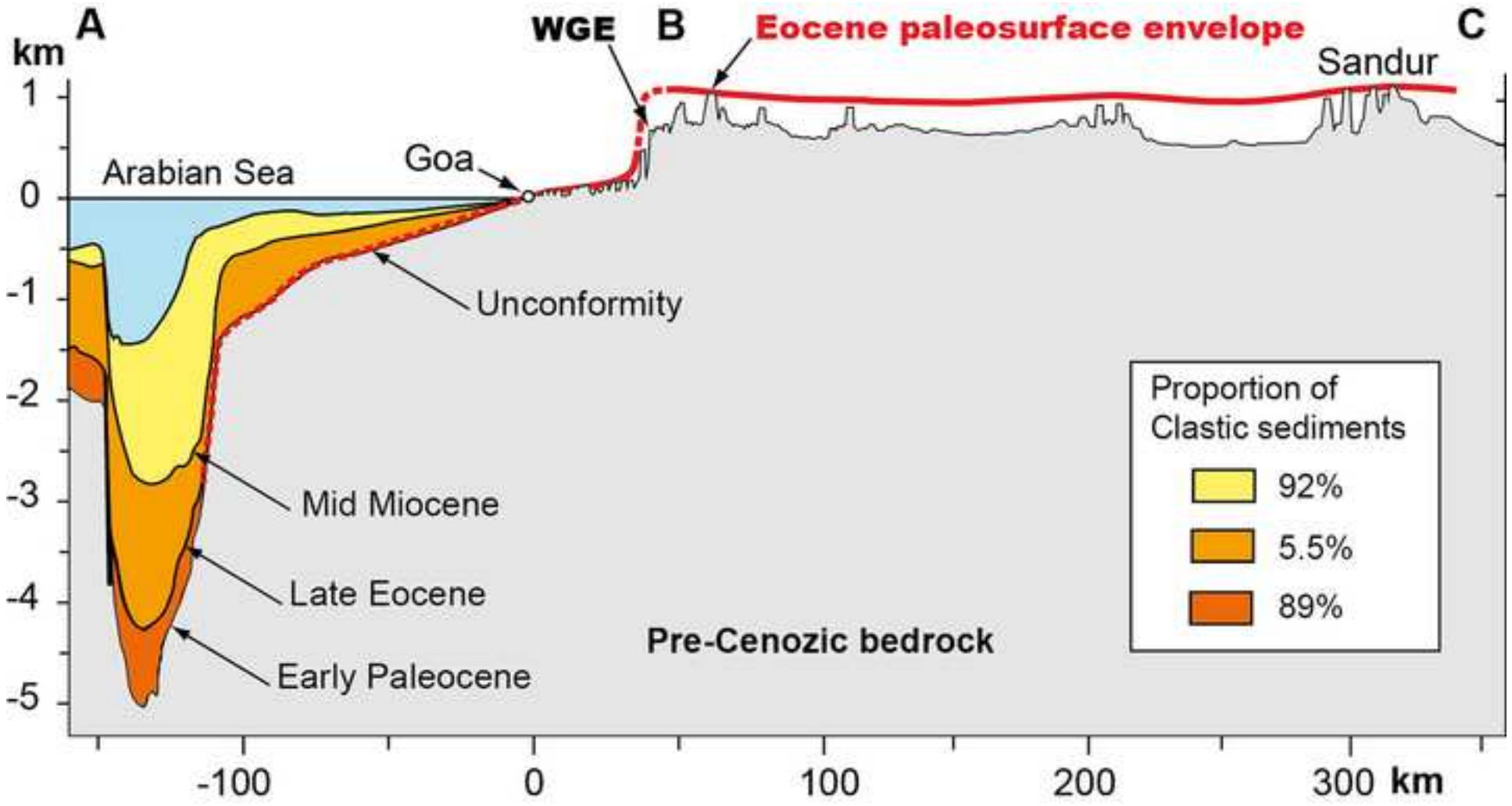

FIGURE 3

Beauvais et al., 2015, Very long term stability of passive margin escarpment constrained by ^{40}Ar-^{39}Ar dating of K-Mn oxides

Supplementary material

Manganiferous ore samples have been sampled in upland Sandur ore deposits (KPA-8: 15° 0' 2.27"N/76° 32' 41.6"E; KMK-2: 14° 59' 48.34"N/76° 34' 40.34"E) and in lowland ore deposits, Naveli (NAV-3: 15° 07' 55.10"N/74° 09' 49.72''E; NAV-4: 15° 08' 07.12"N/74° 09' 32.26''E), and Caurem (CAU-1: 15° 07' 2.19"N/74° 08' 39.66"E; CAU-3: 15° 07' 3.47"N/74° 08' 38.97"E).

Cryptomelane grains were separated from 300-500 μm thick slabs by hand picking. The separated grains were ultrasonically cleaned in absolute ethanol and conditioned in aluminium foil packets, to be irradiated for 50 hours in the TRIGA Mark-II reactor of Pavia University (Italia). The Factor J was determined from the analysis of the standard Taylor Creek Rhyolite sanidine-2 (TCRs-2) monitor, with an age of 28 ± 0.08 Ma (Baksi et al., 1996). The standard was analyzed after every ten unknown samples. After a two-month "cooling" period, the irradiated cryptomelane grains were loaded in a double vacuum Staudacher-type furnace for step heating Ar isotopes measurements. The furnace temperature was calibrated by means of a classical thermocouple, and the gas purification was accomplished using a cold trap with liquid air and Al–Zr AP10 getters (one hot, one cold) for 8 minutes before the introduction into the VG3600 mass spectrometer. One minute was allowed for equilibration before analysis. ^{40}Ar and ^{39}Ar were measured on a Faraday cup with a resistor of 10^{11} ohm, while ^{39}Ar, ^{38}Ar, ^{37}Ar, and ^{36}Ar were analyzed using a scintillator and photomultiplier after interaction on a Daly plate. The analytical data are reported in data repositories (Figures DR1 and Table DR2), and the errors are quoted at the 1σ level. Plateau ages are calculated from at least three consecutive ^{39}Ar release steps comprising up to 50% of total $^{39}Ar_K$ released and overlapping at the 2σ confidence level (Fleck et al., 1977). Isochrone

ages are accepted when mean square weighted deviation (MSWD) is less than 2.5 and the $^{40}Ar/^{36}Ar$ intercept within 2σ from the $(^{40}Ar/^{36}Ar)_{atm}$ value of 298.56 ± 0.31 (Lee et al., 2006 ; Renne et al., 2009).

References cited

Baksi, A.K., Archibald, D.A., and Farrar, E., 1996, Intercalibration of $^{40}Ar^{39}Ar$ dating standards: Chem. Geol., v. 129, p. 307-324.

Fleck, R.J., Sutter, J.F., and Elliot, D.H., 1977, Interpretation of discordant $^{40}Ar/^{39}Ar$ age-spectra of mesozoic tholeiites from Antarctica: Geochim. Cosmochim. Acta, v. 41, p. 15-32.

Lee J-Y, Marti, K., Severinghaus, J.P., Kawamura, K., Yoo, H.S., Lee, J.B., and Kim, J.S., 2006, A redetermination of the isotopic abundances of atmospheric Ar: Geochim. Cosmochim. Acta, v. 70, p. 4507–4512.

Renne, P.R., Cassata, W.S., and Morgan, L.E., 2009, The isotopic composition of atmospheric argon and 40Ar/39Ar geochronology: time for a change: Quat. Geochron., v. 4, p. 288-298.

Figure. DR1. ^{39}Ar releasing spectra showing well defined plateau ages with K/Ca (grey) and Ar* (black) step curves (left) and inverse isochrone diagrams (right) of cryptomelane grains from the open pits samples of **(A)** Sandur **(B)** Naveli and **(C)** Caurem Mn ore deposits (MSWD = mean square weighted deviation).

Tables. DR2-DR3. Analytical results obtained for highland and lowland cryptomelane grains, either from Laser energy (spectrometer Argus IV) or double vacuum Staudacher-type furnace temperature, T °C, (spectrometer VG 3600) for each irradiated crypromelane grain. The

concentrations of ^{36}Ar, ^{37}Ar, ^{38}Ar, ^{39}Ar and ^{40}Ar with their respective 1σ error are provided for each step heating. The amount of $^{40}Ar^*$ (%), of ^{39}Ar released (%^{39}Ar) and the K/Ca ratio (derived from $^{39}Ar/^{37}Ar$) are also given. Finally, this table show ratios $^{40}Ar^*/^{39}Ar_k$ used to determine the corresponding apparent ages, which are presented in the last column with their associated 2σ error. The different J-Factor values are also provided for each irradiated grains.

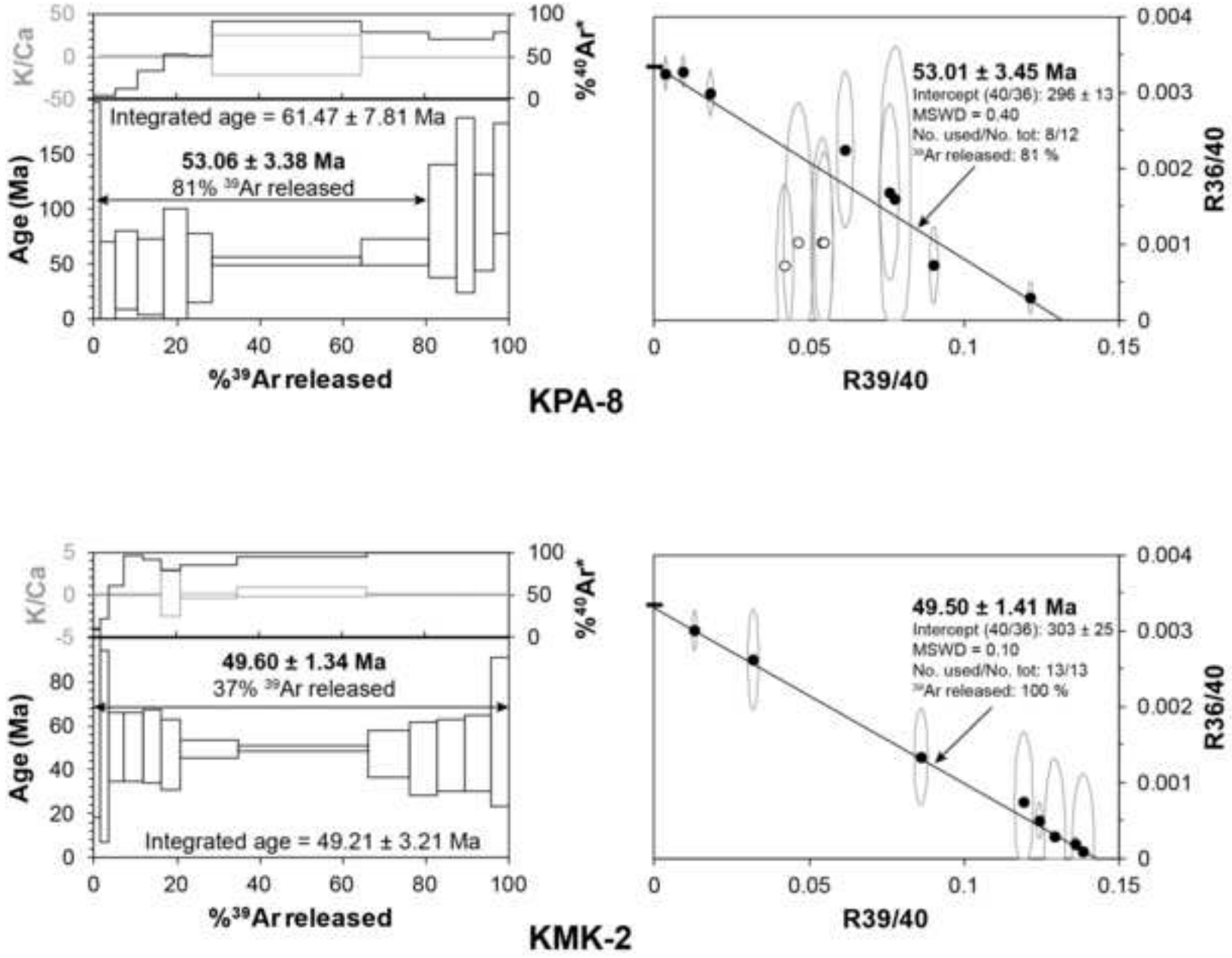

Figure. DR1- A

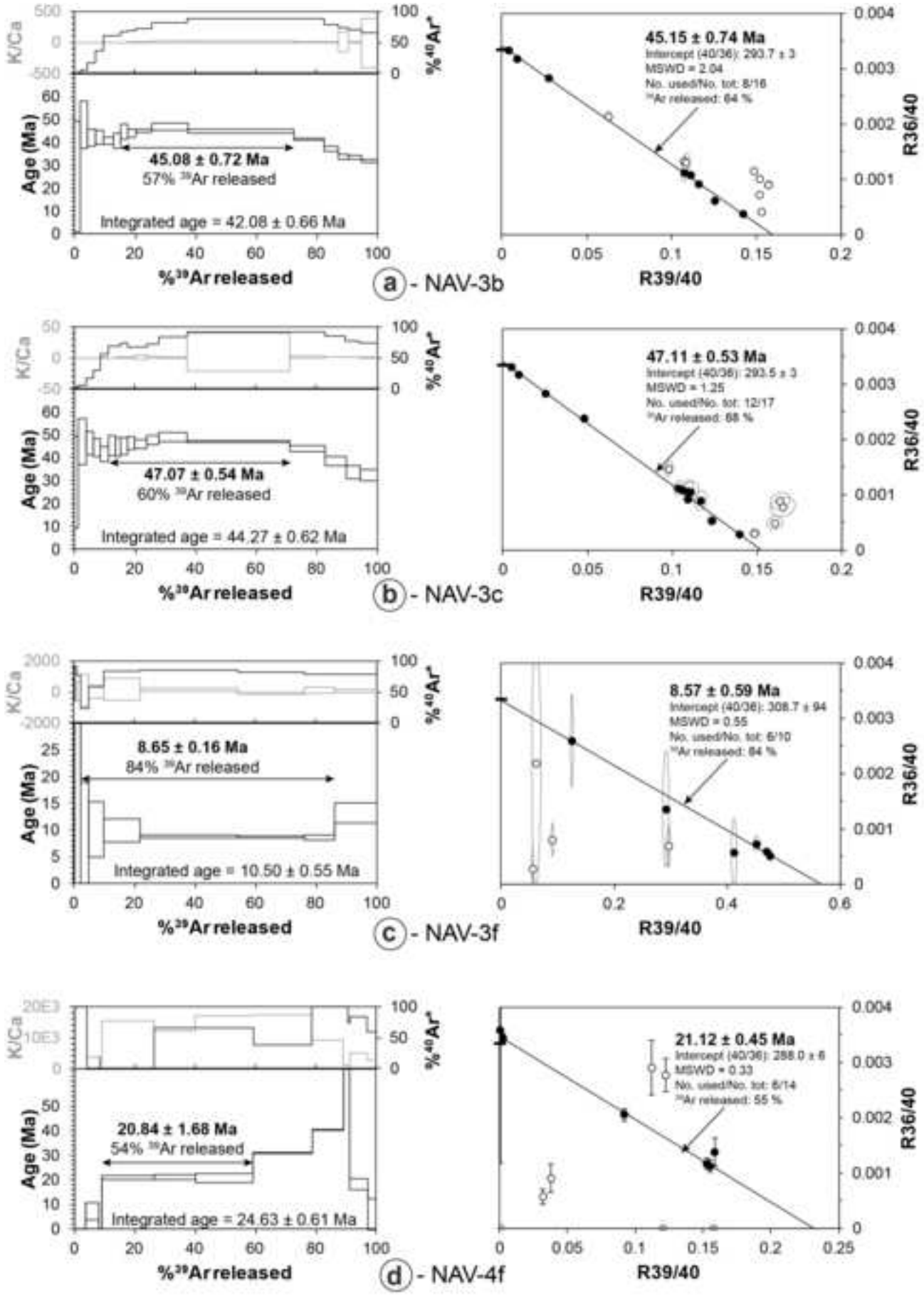

FIGURE. DR1-B

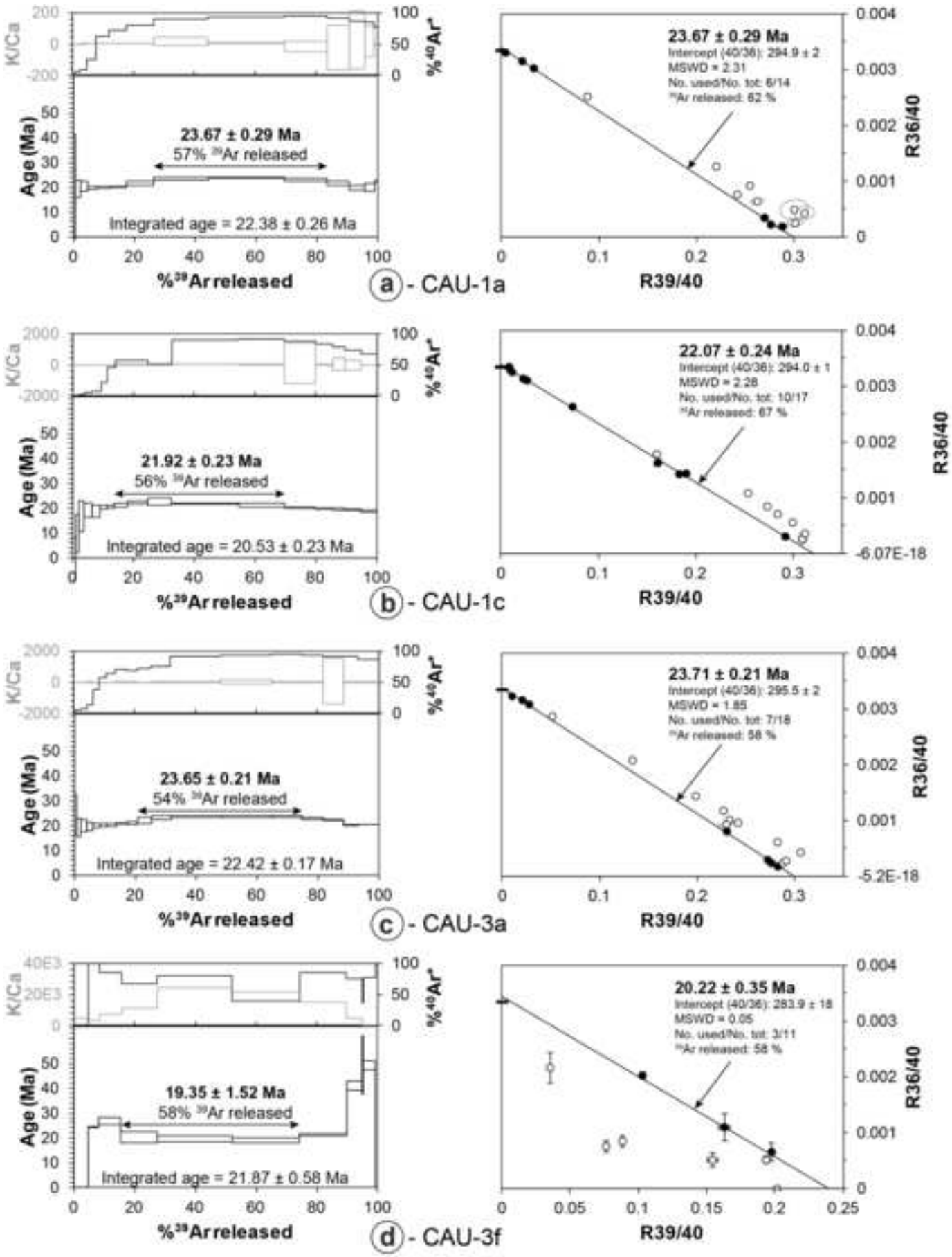

FIGURE. DR1-C

Click here to download Supplemental file Supl. file_Table. DR2.xlsx

KMK-2 J = 0.00402950 ± 0.00000363

Relative Abundances			36Ar [V]	%1σ	37Ar [V]	%1σ	38Ar [V]	%1σ	39Ar [V]	%1σ	40Ar [V]	%1σ	40(r)/39(k) ± 2σ	Age ± 2σ (Ma)	40Ar(r) (%)	39Ar(k) (%)	K/Ca ± 2σ
48_KMK-2	4 °C	4	1.1839652	0.511	231.8581	72.426	0.3215167	6.386	4.95915	0.668	371.0028	0.252	8.52452 ± 6.07881	61.07 ± 42.82	11.01	1.46	0.0089 ± 0.0129
49_KMK-2	4 °C	4	0.5680986	0.691	134.9113	172.430	0.2579779	9.837	6.52910	0.550	201.6829	0.468	7.03545 ± 6.19151	50.55 ± 43.87	22.43	1.95	0.0205 ± 0.0707
51_KMK-2	5 °C	4	0.2762329	1.149	265.9626	60.978	0.2666950	9.407	13.01527	0.628	148.9358	0.627	7.00618 ± 2.17753	50.34 ± 15.43	60.32	3.89	0.0207 ± 0.0253
52_KMK-2	5 °C	4	0.0984086	3.023	303.8510	62.665	0.2356036	8.707	15.12151	0.301	107.7680	0.866	7.00719 ± 2.19461	50.35 ± 15.55	96.89	4.53	0.0211 ± 0.0264
53_KMK-2	5 °C	4	0.0963079	3.187	216.0023	93.560	0.2716634	7.769	14.61645	0.193	114.3836	0.819	7.05201 ± 2.34370	50.67 ± 16.61	91.08	4.49	0.0288 ± 0.0539
55_KMK-2	6 °C	4	0.0999899	2.979	29.7181	649.669	0.2428391	8.840	14.53952	0.185	121.8410	0.766	6.52232 ± 2.27418	46.91 ± 16.15	77.72	4.41	0.2101 ± 2.7294
56_KMK-2	6 °C	4	0.1380666	2.228	-169.60	90.823	0.6075632	4.609	44.83913	0.130	369.8846	0.260	6.83980 ± 0.57628	49.16 ± 4.09	84.95	13.95	-0.1140 ± 0.2071
57_KMK-2	6 °C	4	0.1912850	1.639	143.1068	85.817	1.3379733	1.752	100.95234	0.115	758.6071	0.123	6.92242 ± 0.20665	49.75 ± 1.46	94.03	31.30	0.3030 ± 0.5201
4_KMK-2_	7 °C	4	0.0770691	11.247	294.5770	98.924	0.4479906	5.973	33.31179	0.128	219.7423	1.161	6.55654 ± 1.48708	47.15 ± 10.56	100.90	10.27	0.0483 ± 0.0956
5_KMK-2_	7 °C	4	0.0584562	14.822	403.3393	72.429	0.2896831	11.745	21.71829	0.152	117.2863	2.176	6.26068 ± 2.35533	45.05 ± 16.74	114.37	6.51	0.0228 ± 0.0331
6_KMK-2_	8 °C	4	0.0724425	12.081	617.6113	48.098	0.3092851	10.266	22.86000	0.140	114.7255	2.224	6.49998 ± 2.29767	46.75 ± 16.31	126.97	6.81	0.0156 ± 0.0150
8_KMK-2_	10 °C	4	0.0912916	9.525	704.0786	40.752	0.3388404	7.878	21.13750	0.219	103.3896	2.469	6.60114 ± 2.41926	47.47 ± 17.17	131.69	6.27	0.0126 ± 0.0103
9_KMK-2_	12 °C	4	0.0525406	16.497	573.1992	66.571	0.2170933	14.152	14.13494	0.357	76.3872	3.342	7.98376 ± 4.79143	57.26 ± 33.83	143.38	4.17	0.0103 ± 0.0137
		Σ	3.0041547	0.734	3748.6166	23.075	5.1447248	1.833	327.73499	0.060	2825.6367	0.223					

KPA-8 J = 0.0039438 ± 0.00000355

Relative Abundances			36Ar [V]	%1σ	37Ar [V]	%1σ	38Ar [V]	%1σ	39Ar [V]	%1σ	40Ar [V]	%1σ	40(r)/39(k) ± 2σ	Age ± 2σ (Ma)	40Ar(r) (%)	39Ar(k) (%)	K/Ca ± 2σ
31_KPA-8l	3 °C		2.8089159	0.536	234.32	130.296	0.6593686	3.542	3.20068	0.820	843.8298	0.072	11.13103 ± 17.59558	77.69 ± 120.21	4.00	1.52	0.0056 ± 0.0145
32_KPA-8l	4 °C		2.6898971	0.550	195.28	150.750	0.6711098	4.116	7.48457	0.411	829.3414	0.068	7.10266 ± 7.13672	49.96 ± 49.51	6.15	3.61	0.0162 ± 0.0488
33_KPA-8l	4 °C	4	1.7738239	0.533	261.41	118.841	0.5120498	5.930	10.48252	0.495	574.4086	0.096	7.18749 ± 5.30643	50.55 ± 36.80	12.60	5.06	0.0169 ± 0.0402
35_KPA-8l	5 °C	4	0.4962284	0.761	97.74	380.046	0.2574942	9.157	13.08041	0.307	212.9395	0.259	5.85080 ± 4.97662	41.25 ± 34.69	34.98	6.40	0.0572 ± 0.4350
36_KPA-8l	5 °C	4	0.2897844	0.903	213.48	232.238	0.2457546	6.535	11.22189	0.282	142.6239	0.386	6.78306 ± 7.64231	47.74 ± 53.08	52.63	5.56	0.0223 ± 0.1035
37_KPA-8l	5 °C	4	0.3112543	0.847	130.12	250.994	0.2640977	12.342	12.42831	0.238	162.4586	0.337	6.60376 ± 4.51844	46.49 ± 31.41	50.14	6.20	0.0408 ± 0.2046
39_KPA-8l	5 °C	4	0.1868086	1.810	23.81	913.916	0.9692660	2.109	71.99564	0.134	593.5181	0.148	7.49733 ± 0.51736	52.69 ± 3.58	90.92	36.17	1.2999 ± 23.7605
40_KPA-8l	6 °C	4	0.0683805	3.439	-745.35	46.385	0.3885421	7.195	32.44277	0.200	364.3965	0.454	8.68685 ± 1.84452	60.91 ± 12.72	76.96	16.22	-0.0190 ± 0.0177
41_KPA-8l	6 °C		0.0430701	2.523	-813.85	69.654	0.1578973	15.361	12.94441	0.371	248.4135	0.063	12.55212 ± 7.34728	87.37 ± 49.93	66.94	6.66	-0.0072 ± 0.0100
43_KPA-8l	6 °C		0.0425698	2.407	-572.74	96.309	0.1136482	26.458	8.10058	0.637	181.0269	0.085	14.35041 ± 11.36444	99.55 ± 76.71	66.08	4.19	-0.0064 ± 0.0123
44_KPA-8l	7 °C		0.0562862	1.242	-483.32	65.192	0.1757371	11.013	9.27267	0.519	174.7342	0.091	12.14450 ± 5.62442	84.60 ± 38.28	66.89	4.84	-0.0086 ± 0.0112
45_KPA-8l	8 °C		0.0601309	1.322	-240.19	109.146	0.1056815	20.501	7.09495	0.579	172.0936	0.089	18.80735 ± 6.36101	129.39 ± 42.23	77.76	3.58	-0.0130 ± 0.0284
		Σ	8.8271500	0.273	-1699.29	77.343	4.5206470	1.934	199.74940	0.087	4499.7847	0.052					

TABLE DR2

Click here to download Supplemental file Supl. file_Table. DR3.xlsx

CAU-1a J=0.00395580±0.0000047! Spectro : ARGUS IV

Relative Abundances		36Ar [fA]	%1s	37Ar [fA]	%1s	38Ar [fA]	%1s	39Ar [fA]	%1s	40Ar [fA]	%1s	40*/39(k) ± 2s	Age ± 2s (Ma)	40Ar* (%)	39Ar(k) (%)	K/Ca ± 2s
18_CAU1A	3.0 %	4.516016	0.477	43.54992	5.860	1.365495	1.126	5.61404	0.644	1360.5627	0.255	2.85746 ± 2.99338	20.28 ± 21.12	1.17	0.60	0.06 ± 0.01
20_CAU1A	3.5 %	2.272683	0.432	36.60379	12.817	0.890510	1.677	15.25865	0.155	717.1486	0.072	2.73215 ± 0.47587	19.39 ± 3.36	5.80	1.65	0.18 ± 0.05
21_CAU1A	4.0 %	2.050184	0.393	34.64924	13.773	0.883057	1.870	22.40054	0.164	673.5708	0.076	2.87059 ± 0.27648	20.37 ± 1.95	9.54	2.42	0.28 ± 0.08
22_CAU1A	4.5 %	0.763622	0.466	18.26025	24.101	0.678404	3.097	26.48788	0.128	41967.0000	0.170	2.80282 ± 0.10697	19.89 ± 0.76	24.66	2.87	0.62 ± 0.30
24_CAU1A	5.0 %	0.235595	1.038	18.60246	23.769	0.653277	2.811	39.92276	0.101	181.5618	0.275	2.81728 ± 0.04966	19.99 ± 0.35	61.93	4.32	0.92 ± 0.44
25_CAU1A	5.3 %	0.191578	1.253	17.25970	27.923	0.768086	2.162	51.32276	0.097	201.9357	0.263	2.84008 ± 0.03928	20.16 ± 0.28	72.16	5.56	1.28 ± 0.72
26_CAU1A	5.6 %	0.210138	3.758	14.00596	25.408	1.143705	1.627	83.77487	0.099	320.1243	1.220	3.07741 ± 0.10942	21.83 ± 0.77	80.52	9.07	2.57 ± 1.32
28_CAU1A	5.9 %	0.214924	8.727	4.18793	83.477	2.219469	2.132	164.39158	0.101	610.8941	0.773	3.31832 ± 0.08947	23.53 ± 0.63	89.29	17.81	16.88 ± 28.21
29_CAU1A	6.2 %	0.200666	9.468	23.74601	29.916	3.053111	1.986	232.17280	0.095	842.4791	0.263	3.36998 ± 0.05313	23.89 ± 0.37	92.86	25.15	4.20 ± 2.54
30_CAU1A	6.5 %	0.085851	12.755	-3.16533	90.190	1.692738	1.080	128.77458	0.096	448.2447	1.051	3.26994 ± 0.08935	23.19 ± 0.63	93.94	13.95	-17.49 ± 31.59
32_CAU1A	6.8 %	0.058090	13.479	-1.21155	291.762	0.891483	3.860	68.16303	0.103	226.8244	1.264	3.06198 ± 0.10910	21.72 ± 0.77	92.02	7.38	-24.19 ± 141.18
33_CAU1A	7.1 %	0.062935	13.683	0.72994	342.136	0.629049	3.290	45.41806	0.111	146.5107	1.637	2.80384 ± 0.15528	19.90 ± 1.10	86.92	4.92	26.75 ± 183.09
34_CAU1A	7.5 %	0.049687	17.355	0.84383	320.119	0.413439	5.188	29.82742	0.126	99.5771	2.409	2.83390 ± 0.23659	20.11 ± 1.67	84.89	3.23	15.20 ± 97.32
36_CAU1A	8.0 %	0.030373	1.549	-1.78502	106.081	0.205951	5.066	9.72380	0.186	40.2830	0.133	3.18423 ± 0.04745	22.58 ± 0.33	76.87	1.05	-2.34 ± 4.97
	S	10.942342	0.383	206.27712	7.297	15.487774	0.664	923.25278	0.037	6170.5939	0.160					

CAU-1c J=0.00395580±0.0000047! Spectro : ARGUS IV

Relative Abundances		36Ar [fA]	%1s	37Ar [fA]	%1s	38Ar [fA]	%1s	39Ar [fA]	%1s	40Ar [fA]	%1s	40(r)/39(k) ± 2s	Age ± 2s (Ma)	40Ar(r) (%)	39Ar(k) (%)	K/Ca ± 2s
06_CAU1C	3.0 %	2.955930	0.415	36.55443	4.950	1.188579	1.545	7.49918	0.219	879.1289	0.049	-0.04320 ± 1.21342	-0.31 ± 8.66	-0.04	0.88	0.09 ± 0.01
08_CAU1C	3.5 %	3.301567	0.406	31.94784	3.601	1.261587	1.337	9.28493	0.281	995.9706	0.048	1.39414 ± 1.07867	9.92 ± 7.66	1.30	1.09	0.12 ± 0.01
09_CAU1C	4.0 %	4.366770	0.407	37.89264	3.444	1.446225	1.452	15.46007	0.135	1336.8954	0.036	2.34966 ± 0.85575	16.69 ± 6.05	2.71	1.81	0.18 ± 0.02
010_CAU1(	4.5 %	2.905542	0.406	29.32351	4.520	1.096971	1.101	21.11387	0.134	922.4625	0.050	2.71663 ± 0.41727	19.28 ± 2.95	6.21	2.48	0.31 ± 0.04
012_CAU1(	5.0 %	2.808190	0.412	21.32195	6.432	1.081115	1.994	24.04572	0.140	900.7403	0.047	2.66030 ± 0.35754	18.89 ± 2.53	7.10	2.83	0.48 ± 0.07
013_CAU1(	5.3 %	0.682495	0.508	7.84246	28.831	0.438070	4.678	18.96641	0.189	257.9112	0.158	2.88154 ± 0.13577	20.45 ± 0.96	21.18	2.23	1.04 ± 0.61
014_CAU1(	5.6 %	0.233447	0.730	11.09798	11.352	0.336339	6.030	20.62905	0.159	129.0176	0.331	2.91325 ± 0.06890	20.67 ± 0.49	46.56	2.43	0.80 ± 0.19
4_CAU1C_	5.9 %	0.285420	2.334	4.93811	52.818	0.611927	5.553	37.44759	0.124	197.2739	0.741	2.99436 ± 0.13332	21.24 ± 0.94	56.84	4.40	3.26 ± 3.45
5_CAU1C_	6.2 %	0.427052	1.686	5.19248	70.435	0.909102	4.496	54.41640	0.102	297.7087	0.237	3.12662 ± 0.08535	22.18 ± 0.60	57.15	6.40	4.51 ± 6.36
6_CAU1C_	6.5 %	0.683213	1.694	17.30755	11.221	1.187802	3.433	66.87030	0.104	415.6859	1.341	3.17908 ± 0.19716	22.55 ± 1.39	51.13	7.86	1.66 ± 0.40
8_CAU1C_	6.8 %	0.207712	5.554	5.09086	41.333	2.817174	1.039	189.33288	0.102	650.6676	0.141	3.10177 ± 0.03826	22.00 ± 0.27	90.25	22.27	15.99 ± 13.28
9_CAU1C_	7.1 %	0.114870	19.203	13.93231	29.290	1.743316	2.087	126.98796	0.106	411.8709	0.669	2.97330 ± 0.11276	21.10 ± 0.80	91.67	14.93	3.92 ± 2.32
10_CAU1C	7.4 %	0.102980	3.803	0.35399	621.535	1.155650	3.393	87.29553	0.114	280.5889	0.325	2.85271 ± 0.03494	20.24 ± 0.25	88.75	10.27	106.04 ± 1318.18
12_CAU1C	7.7 %	0.090989	2.165	-1.95185	133.733	0.698318	2.792	48.22579	0.107	161.5814	0.338	2.77397 ± 0.03523	19.69 ± 0.25	82.79	5.67	-10.62 ± 28.43
13_CAU1C	8.0 %	0.081707	2.296	0.47047	666.908	0.499815	5.382	32.40767	0.108	114.4076	0.478	2.76912 ± 0.05165	19.65 ± 0.36	78.44	3.81	29.62 ± 395.08
14_CAU1C	9.0 %	0.141869	1.402	-0.53409	444.453	0.695800	2.822	45.50024	0.106	166.9138	0.328	2.72679 ± 0.03747	19.36 ± 0.26	74.33	5.35	-36.63 ± 325.65
16_CAU1C	12.0 %	0.191802	1.179	-6.29791	38.434	0.747016	2.177	45.00317	0.108	177.7849	0.307	2.65605 ± 0.04085	18.86 ± 0.29	67.24	5.29	-3.07 ± 2.37
	S	19.581555	0.218	214.48272	4.536	17.914806	0.623	850.48676	0.035	8296.6101	0.081					

CAU-3a J=0.00395580±0.0000047! Spectro : ARGUS IV

Relative Abundances		36Ar [fA]	%1s	37Ar [fA]	%1s	38Ar [fA]	%1s	39Ar [fA]	%1s	40Ar [fA]	%1s	40*/39(k) ± 2s	Age ± 2s (Ma)	40Ar* (%)	39Ar(k) (%)	K/Ca ± 2s
18_CAU3A	3.5 %	2.2527018	0.466	17.64813	36.203	0.714955	2.749	7.1070	0.289	695.7188	0.189	3.46778 ± 1.12519	24.58 ± 7.92	3.54	0.70	0.17 ± 0.13
20_CAU3A	4.0 %	2.1473180	0.427	15.14025	28.344	0.854097	3.415	14.0449	0.161	677.8913	0.163	2.70444 ± 0.50482	19.20 ± 3.56	5.60	1.38	0.40 ± 0.23
21_CAU3A	4.5 %	2.2260178	0.389	22.16793	18.988	0.862905	2.126	20.0461	0.110	719.9477	0.153	2.84873 ± 0.34578	20.22 ± 2.44	7.93	1.97	0.39 ± 0.15
22_CAU3A	5.0 %	1.1741790	0.560	3.07897	190.743	0.616350	3.261	21.0334	0.122	408.6987	0.286	2.76716 ± 0.24398	19.64 ± 1.72	14.24	2.07	2.94 ± 11.21
24_CAU3A	5.3 %	0.3310181	1.105	14.55382	29.578	0.406194	5.047	20.9485	0.142	156.9493	0.196	2.82593 ± 0.11763	20.06 ± 0.83	37.70	2.06	0.62 ± 0.37
25_CAU3A	5.6 %	0.1839528	1.726	11.83707	39.537	0.427402	5.587	24.8448	0.136	125.2538	0.253	2.86316 ± 0.08810	20.32 ± 0.62	56.77	2.45	0.90 ± 0.72
26_CAU3A	5.9 %	0.1562779	2.069	-6.68326	67.802	0.428279	4.903	30.3017	0.121	133.8858	0.225	2.84952 ± 0.07246	20.22 ± 0.51	64.50	2.99	-1.95 ± 2.65
28_CAU3A	6.2 %	0.1465956	2.680	4.39217	88.759	0.555135	3.871	36.4632	0.111	151.0139	0.473	2.94214 ± 0.07815	20.88 ± 0.55	71.03	3.59	3.57 ± 6.34
29_CAU3A	6.5 %	0.1582600	2.540	9.51032	43.392	0.537045	2.946	35.6433	0.105	153.2633	0.456	2.98811 ± 0.08107	21.20 ± 0.57	69.48	3.51	1.61 ± 1.40
30_CAU3A	6.8 %	0.1910077	1.264	12.70945	23.217	0.664209	2.160	46.0625	0.106	200.5556	1.876	3.13061 ± 0.16705	22.20 ± 1.18	71.89	4.54	1.56 ± 0.73
32_CAU3A	7.2 %	0.2322562	3.873	9.80682	28.757	0.933880	4.641	65.1650	0.152	283.3798	0.571	3.28815 ± 0.09724	23.31 ± 0.69	75.60	6.42	2.86 ± 1.66
33_CAU3A	7.5 %	0.1868738	8.660	3.36755	68.413	2.260665	1.948	167.8381	0.088	617.6648	0.075	3.33978 ± 0.05822	23.68 ± 0.41	90.75	16.54	21.43 ± 29.37
34_CAU3A	7.8 %	0.1520246	2.920	2.24741	171.304	2.226168	0.771	169.8242	0.073	616.4084	0.579	3.35390 ± 0.04533	23.78 ± 0.32	92.40	16.73	32.49 ± 111.35
36_CAU3A	8.5 %	0.0639352	13.956	2.48021	130.478	1.305095	3.360	99.4785	0.121	352.4664	0.129	3.34377 ± 0.05523	23.71 ± 0.39	94.37	9.80	17.25 ± 45.03
37_CAU3A	9.0 %	0.0590189	15.080	-2.56009	130.499	0.978539	4.451	72.3497	0.139	252.4294	0.179	3.23266 ± 0.07548	22.92 ± 0.53	92.65	7.13	-12.15 ± 31.73
38_CAU3A	9.0 %	0.0655049	4.850	0.42226	1074.174	0.934827	2.873	66.3406	0.088	228.2513	0.256	3.13667 ± 0.03605	22.25 ± 0.25	91.17	6.54	67.56 ± 1451.36
40_CAU3A	10.0 %	0.0718457	3.673	4.55087	53.924	0.792799	3.688	49.2345	0.126	161.2931	0.255	2.83879 ± 0.03787	20.15 ± 0.27	86.65	4.85	4.65 ± 5.03
41_CAU3A	12.0 %	0.1531753	1.703	10.99301	31.140	1.058174	3.460	68.2344	0.102	242.1234	0.171	2.88269 ± 0.02816	20.46 ± 0.20	81.23	6.72	2.67 ± 1.68
	S	9.9519632	0.306	135.66289	12.797	16.556718	0.744	1014.9604	0.030	6177.1947	0.099					

TABLE DR3

NAV-3b J=0.00402950±0.00000 Spectro : ARGUS IV

Relative Abundances		36Ar [V]	%1s	37Ar [V]	%1s	38Ar [V]	%1s	39Ar [V]	%1s	40Ar [V]	%1s	40*/39(k) ± 2s	Age ± 2s (Ma)	40Ar* (%)	39Ar(k) (%)	K/Ca ± 2s
9_NAV-3B	4.0%	24.071859	0.571	974.8500	3.800	6.452027	0.489	29.2382	0.264	7129.981	0.048	3.49467 ± 3.35953	25.29 ± 24.14	1.40	1.97	0.013 ± 0.001
10_NAV-3	5.0%	11.580366	0.574	648.5615	5.972	3.480601	0.789	32.7046	0.237	3580.652	0.083	6.62952 ± 1.45997	47.67 ± 10.36	5.97	2.23	0.021 ± 0.003
12_NAV-3	5.5%	3.903645	0.616	440.0984	9.459	1.590267	1.424	37.1487	0.213	1332.082	0.227	5.85733 ± 0.52065	42.18 ± 3.71	16.19	2.55	0.036 ± 0.007
13_NAV-3	6.0%	1.468001	0.768	261.4635	33.774	0.998112	1.998	41.1356	0.212	651.098	0.458	5.84172 ± 0.43820	42.07 ± 3.12	36.74	2.83	0.067 ± 0.045
14_NAV-3	6.3%	0.626130	1.393	225.9253	12.936	0.901243	2.375	45.2578	0.204	420.622	0.721	5.64217 ± 0.21635	40.65 ± 1.54	60.49	3.12	0.086 ± 0.022
16_NAV-3	6.6%	0.450185	1.795	79.9672	112.109	0.649674	3.459	35.6219	0.236	327.276	0.914	5.64410 ± 0.48233	40.67 ± 3.44	61.33	2.46	0.191 ± 0.429
17_NAV-3	6.9%	0.391032	2.037	142.1313	56.491	0.620744	3.355	33.6207	0.222	311.508	0.958	6.19825 ± 0.47011	44.61 ± 3.34	66.69	2.32	0.101 ± 0.115
18_NAV-3	7.2%	0.383583	2.104	36.5946	75.686	0.679554	3.692	38.3892	0.211	344.616	0.885	6.10043 ± 0.23878	43.91 ± 1.70	67.91	2.65	0.451 ± 0.682
20_NAV-3	7.5%	0.617538	1.367	-31.8060	80.778	1.253744	1.678	78.9865	0.162	680.972	0.443	6.26551 ± 0.11657	45.09 ± 0.83	72.70	5.46	-1.068 ± 1.726
21_NAV-3	7.8%	0.845306	5.636	17.6699	160.546	2.497727	1.983	170.3464	0.155	1357.707	0.693	6.50367 ± 0.20211	46.78 ± 1.44	81.59	11.77	4.145 ± 13.310
22_NAV-3	8.1%	1.375291	5.032	30.9040	95.668	6.908670	1.099	507.1068	0.144	3567.849	0.541	6.23009 ± 0.11296	44.84 ± 0.80	88.55	35.05	7.056 ± 13.500
24_NAV-3	8.4%	0.427832	1.741	123.3786	33.397	1.980591	1.118	144.0581	0.143	941.179	0.185	5.72255 ± 0.06529	41.22 ± 0.47	87.54	9.95	0.502 ± 0.335
25_NAV-3	8.7%	0.347291	2.174	49.9188	77.368	1.043066	2.383	69.6635	0.161	458.658	0.478	5.16493 ± 0.13201	37.25 ± 0.94	78.41	4.81	0.600 ± 0.928
26_NAV-3	9.0%	0.273815	2.708	2.3805	946.327	0.670710	3.440	47.3429	0.189	301.250	0.728	4.64885 ± 0.15548	33.56 ± 1.11	73.06	3.27	8.551 ± 161.850
28_NAV-3	10.0%	0.424388	1.799	43.4034	57.291	0.923435	2.180	61.7075	0.173	406.348	0.539	4.60544 ± 0.12494	33.25 ± 0.89	69.90	4.26	0.611 ± 0.700
29_NAV-3	12.0%	0.597971	1.363	-2.0230	1208.846	1.190922	2.100	76.8151	0.165	517.295	0.424	4.42211 ± 0.10297	31.94 ± 0.74	65.67	5.31	-16.328 ± 394.761
	S	47.784230	0.373	3043.4182	6.214	31.841089	0.397	1449.1435	0.060	22329.092	0.107					

NAV-3c J=0.00402950±0.00000 Spectro : ARGUS IV

Relative Abundances		36Ar [V]	%1s	37Ar [V]	%1s	38Ar [V]	%1s	39Ar [V]	%1s	40Ar [V]	%1s	40(r)/39(k) ± 2s	Age ± 2s (Ma)	40Ar(r) (%)	39Ar(k) (%)	K/Ca ± 2s
30_NAV-3	4.0%	8.752647	0.596	426.7565	8.165	2.514326	1.690	13.5829	0.722	2603.852	0.128	4.05000 ± 2.78278	29.27 ± 19.95	2.06	1.15	0.013 ± 0.002
33_NAV-3	5.0%	11.214253	0.583	585.3519	5.546	3.508387	1.328	33.1208	0.329	3477.948	0.095	6.53924 ± 1.40857	47.03 ± 10.00	6.15	2.83	0.024 ± 0.003
34_NAV-3	5.5%	2.908345	0.749	363.0345	9.858	1.302245	2.816	25.2080	0.399	989.550	0.338	6.44893 ± 0.68821	46.39 ± 4.89	16.26	2.16	0.030 ± 0.006
35_NAV-3	6.0%	1.394728	1.125	296.6431	15.241	0.865514	4.489	26.5601	0.387	549.448	0.614	6.16229 ± 0.54708	44.35 ± 3.89	29.55	2.28	0.038 ± 0.012
37_NAV-3	6.3%	0.530153	2.671	210.5173	22.268	0.707024	4.914	31.4310	0.456	319.566	1.060	5.77253 ± 0.43768	41.58 ± 3.12	56.50	2.71	0.064 ± 0.028
38_NAV-3	6.6%	0.335936	4.083	277.1481	24.569	0.528844	6.699	26.4947	0.450	241.116	1.412	6.28306 ± 0.60876	45.21 ± 4.33	68.52	2.28	0.041 ± 0.020
39_NAV-3	6.9%	0.241142	5.628	141.6432	27.439	0.412575	9.544	21.1454	1.127	190.018	1.741	6.20784 ± 0.60618	44.68 ± 4.31	68.74	1.82	0.064 ± 0.035
41_NAV-3	7.2%	0.242656	5.559	143.1868	33.818	0.448551	8.689	26.2855	0.391	224.302	1.491	6.28464 ± 0.51255	45.22 ± 3.64	73.36	2.27	0.079 ± 0.053
42_NAV-3	7.5%	0.329281	4.115	92.9742	36.342	0.553563	6.936	27.9930	0.392	269.873	1.226	6.45414 ± 0.43010	46.43 ± 3.05	66.78	2.42	0.129 ± 0.094
43_NAV-3	7.8%	0.479685	2.867	19.0977	187.128	0.831439	4.518	46.1147	0.251	435.650	0.758	6.40131 ± 0.26571	46.05 ± 1.89	67.74	4.00	1.038 ± 3.885
45_NAV-3	8.1%	0.382928	3.562	27.6454	116.220	0.714079	5.614	44.3478	0.257	406.026	0.814	6.65059 ± 0.26851	47.82 ± 1.91	72.61	3.84	0.689 ± 1.603
46_NAV-3	8.3%	0.441581	7.202	-103.9544	75.409	1.527758	2.373	108.2819	0.178	879.165	0.975	6.81805 ± 0.26662	49.01 ± 1.89	84.03	9.39	-0.448 ± 0.676
47_NAV-3	8.6%	0.825150	3.863	17.7697	164.163	5.198367	0.801	390.9425	0.145	2804.071	0.284	6.54328 ± 0.06727	47.06 ± 0.48	91.22	33.89	9.460 ± 31.059
4_NAV-3C	9.0%	0.296675	10.789	66.4975	76.241	1.840361	1.671	134.9982	0.165	909.669	0.845	6.12346 ± 0.19278	44.08 ± 1.37	90.84	11.70	0.873 ± 1.331
5_NAV-3C	9.5%	0.274793	9.852	105.6833	37.942	1.096781	2.486	79.8466	0.224	497.948	1.437	5.32747 ± 0.28379	38.41 ± 2.02	85.34	6.91	0.325 ± 0.246
6_NAV-3C	10.0%	0.265903	10.089	38.1470	42.728	0.770335	2.495	53.8095	0.283	325.930	2.196	4.65000 ± 0.40155	33.57 ± 2.87	76.73	4.66	0.606 ± 0.518
8_NAV-3C	12.0%	0.370818	7.520	48.8411	48.762	1.023809	2.959	65.5177	0.249	401.063	1.788	4.50543 ± 0.34034	32.53 ± 2.44	73.56	5.68	0.577 ± 0.562
	S	29.286675	0.408	2756.9828	6.462	23.843957	0.634	1155.6803	0.071	15525.196	0.140					

NAV-3f J=0.00272700±0.00000 Spectro : VG 3600

Relative Abundances		36Ar [V]	%1s	37Ar [V]	%1s	38Ar [V]	%1s	39Ar [V]	%1s	40Ar [V]	%1s	40(r)/39(k) ± 2s	Age ± 2s (Ma)	40Ar(r) (%)	39Ar(k) (%)	K/Ca ± 2s
33260_AR	600 °C	0.0000303	53.662	0.0003365	92.443	0.0000662	26.204	0.0008544	5.743	0.0137850	2.924	5.68804 ± 11.30657	27.83 ± 54.90	35.25	0.15	1 ± 2
33261_AR	650 °C	0.0000194	75.313	0.0004149	74.920	0.0001216	13.749	0.0038414	0.692	0.0686538	0.572	16.37933 ± 2.27331	79.02 ± 10.73	91.64	0.66	4 ± 6
33262_AR	700 °C	0.0000745	19.418	0.0000597	521.472	0.0001942	8.529	0.0083573	0.612	0.0925542	0.431	8.43301 ± 1.03260	41.11 ± 4.98	76.15	1.44	60 ± 628
33263_AR	750 °C	0.0003261	15.991	0.0000765	589.195	0.0003058	8.150	0.0156988	0.216	0.1257348	0.765	1.86222 ± 1.96744	9.16 ± 9.65	23.25	2.70	88 ± 1040
33264_AR	800 °C	0.0001342	38.761	-0.0001787	252.192	0.0004710	5.334	0.0288385	0.219	0.0990994	0.956	2.05119 ± 1.06820	10.09 ± 5.24	59.69	4.95	-69 ± 350
33265_AR	850 °C	0.0000968	53.933	0.0001908	236.068	0.0010055	3.966	0.0689251	0.184	0.1679506	0.563	2.01224 ± 0.44874	9.90 ± 2.20	82.58	11.84	155 ± 733
33266_AR	900 °C	0.0002073	10.139	0.0007232	42.946	0.0023209	1.764	0.1894340	0.207	0.3999653	0.176	1.77859 ± 0.06645	8.75 ± 0.33	84.24	32.53	113 ± 97
33267_AR	950 °C	0.0001615	4.771	-0.0005931	35.101	0.0012941	1.698	0.1271947	0.164	0.2720278	0.281	1.75335 ± 0.03830	8.63 ± 0.19	81.98	21.84	-92 ± 65
33268_AR	1000 °C	0.0000944	9.413	0.0002402	87.036	0.0008270	2.667	0.0582583	0.180	0.1295069	0.491	1.73497 ± 0.09302	8.54 ± 0.46	78.05	10.00	104 ± 182
33270_AR	1450 °C	0.0001905	27.384	0.0005923	76.000	0.0010664	2.254	0.0809093	0.187	0.2736496	0.432	2.67738 ± 0.38234	13.15 ± 1.87	79.16	13.89	59 ± 89
	S	0.0013351	8.254	0.0018623	60.878	0.0076728	1.084	0.5823119	0.087	1.6429275	0.150					

TABLE DR3 (continued)

Step	Temperatur	40Ar/39Ar	38Ar/39Ar	37Ar/39Ar	36Ar/39Ar	39Ar	%39Ar	%40Ar*	40Ar*/39K	Age	± s.d.
NAV-4f	°C				(E-3)	(E-14)	released			Ma	
Spectro : VG 3600						moles					
J= 0.002727											
1	350	233329.16	1.04	66.39745	1039.77	0	0	99.87	0	0	± 0
2	450	477.918	0.409	0.01935	1647.584	0.015	3.91	-1.88	-8.96	0	± 0
3	550	8.185	0.118	0.0005	22.722	0.016	8.2	17.72	1.45	7.121	± 3.503
4	600	1644181.3	1.04	66.39745	5898367.2	0	8.2	-6.01	-103237.8	0	± 0
5	650	8.153	0	0.00269	77.269	0.003	9.01	-180.3	-14.7	0	± 0
6	700	6.563	0.021	0.00012	7.719	0.067	26.42	64.94	4.26	20.848	± 0.988
7	750	6.456	0.008	0.00016	7.304	0.052	40.09	66.26	4.28	20.923	± 1.073
8	800	10.924	0.015	0.00011	22.598	0.073	59.13	38.69	4.23	20.676	± 1.731
9	850	6.353	0.014	0.00011	0.002	0.075	78.77	99.68	6.33	30.89	± 0.089
10	900	8.322	0.012	0.00021	0.003	0.039	89.07	99.75	8.3	40.385	± 0.211
11	950	26.545	0.032	0.00157	24.211	0.005	90.45	72.97	19.37	92.865	± 18.47
12	1000	31.473	0	0.00246	18.469	0.003	91.33	82.6	26	123.561	± 8.969
13	1200	6.321	0.002	0.00038	8.767	0.022	97.05	58.7	3.71	18.162	± 2.383
14	1450	8.936	0	0.00073	25.99	0.011	100	13.83	1.24	6.07	± 6.384

Step	Temperatur	40Ar/39Ar	38Ar/39Ar	37Ar/39Ar	36Ar/39Ar	39Ar	%39Ar	%40Ar*	40Ar*/39K	Age	± s.d.
CAU-3f	°C				(E-3)	(E-14)	released			Ma	
Spectro : VG 3600						moles					
J= 0.002727											
1	550	5.946	0.211	0.00042	27.703	0.019	4.68	-38	-2.26	0	± 0
2	600	4.964	0.071	0.00056	0.009	0.014	8.2	99.54	4.94	24.146	± 0.216
3	650	6.494	0.026	0.00027	3.348	0.029	15.57	84.46	5.49	26.786	± 1.404
4	700	6.145	0.021	0.00017	6.785	0.047	27.41	67.05	4.12	20.159	± 2.29
5	750	5.065	0.02	0.00008	3.36	0.097	52.01	80	4.05	19.826	± 1.234
6	800	9.738	0.021	0.00009	19.76	0.088	74.3	39.84	3.88	18.985	± 0.934
7	850	5.171	0.02	0.00013	2.684	0.061	89.72	84.27	4.36	21.315	± 0.494
8	950	11.343	0.048	0.00039	9.709	0.02	94.84	74.53	8.45	41.119	± 1.734
9	1000	28.501	0	0.00398	61.908	0.002	95.34	35.75	10.19	49.439	± 11.841
10	1200	13.136	0.009	0.53894	10.137	0.015	99.15	77.29	10.16	49.29	± 1.805
11	1450	52.209	0	30714.419	59.822	0.003	100	99.96	-99.93	0	± 0

TABLE DR3 (continued)